



Modeling the efficiency of TiO₂ photocatalytic degradation of MTBE in contaminated water: a support vector regression approach

T. A. Oyehan¹ · M. A. Liadi¹ · I. O. Alade²

© Springer Nature Switzerland AG 2019

Abstract

Methyl tert-Butyl Ether (MTBE) is one of the common environmental contaminants that pose severe risks to human health and the environment. Due to the detrimental effects of MTBE, many efforts have been devoted towards decontamination of wastewater containing MTBE. Most of the reports on the treatment of MTBE are experimental based, which requires studying the effect of several factors such as dosage of the photocatalyst, pH of the medium, the initial concentration of contaminant and the contact time on degradation efficiency in MTBE contaminated waters. Although, this approach is highly dependable and often leads to new insights. However, because the degradation efficiency is influenced by multiple factors, performing experiments to investigate the effect of these factors often increases the experimental burden, thus requiring more time and materials consumption to achieve desirable results. Herein, we propose a computational intelligent strategy to mitigate these challenges. In this contribution, the degradation efficiencies of MTBE in the presence of TiO₂/UV were modeled under various experimental conditions using the support vector regression model. The model was built using experimental data comprising of inputs such as TiO₂ dose, initial MTBE concentration, UV wavelength and contact time. Remarkably, the developed model exhibits significant accuracy as determined from the values of correlation coefficient (98.27%) and root means square error (5.53). In addition, it was determined that the achievable optimum conditions for degradation of 0.5–100 ppm MTBE-contaminated water were 2.4 g/L of TiO₂ dose with UV radiation, a solution pH of 3 and treatment time of 2 h. This study will be useful in the experimental design of treatment for MTBE, consequently reducing the time spent on running experiments and at the same time ensuring efficient use of resources for treatment of MTBE contaminated water.

Keywords MTBE · Photo-catalysis · UV/TiO₂ · Support vector regression

1 Introduction

Methyl tert-Butyl Ether (MTBE) is one of the common oxygenates used as an anti-knock agent to supplant environmentally unsafe tetraethyl lead (TEL) in gasoline since 1979 in the US [1–3]. Following the global ban of TEL by year 2000s, the use of MTBE as a cheap alternative fuel additive became widespread worldwide. MTBE is released

into groundwater aquifer and surface water through leaks from underground storage tanks and through a direct spill of MTBE-containing gasoline. The prevalence of MTBE in water resources portends significant challenges to the safety of drinking water [4–6]. This problem is worsened because of MTBE's uniquely low Henry's constant, high water solubility and its inherently poor in situ anaerobic biodegradability [1, 7]. The ingestion of MTBE via

Electronic supplementary material The online version of this article (<https://doi.org/10.1007/s42452-019-0417-4>) contains supplementary material, which is available to authorized users.

✉ T. A. Oyehan, tajudeenoyehan@kfupm.edu.sa | ¹Geosciences Department (Environmental Program), College of Petroleum Engineering and Geosciences (CPG), King Fahd University of Petroleum and Minerals (KFUPM), Dhahran 31261, Saudi Arabia. ²KFUPM Business School, King Fahd University of Petroleum and Minerals (KFUPM), Dhahran 31261, Saudi Arabia.

SN Applied Sciences (2019) 1:386 | <https://doi.org/10.1007/s42452-019-0417-4>

Received: 16 January 2019 / Accepted: 26 March 2019 / Published online: 2 April 2019

consumption of contaminated water or any other route has severe health consequences. For instance, eye and skin irritancy in human have been linked genotoxically with the long exposure to MTBE [5, 8, 9]. Also, MTBE has been reported to induce mutagenic breakages of DNA strands and modification of oxidative base pair [10]. In lower animals, MTBE causes depression and disruption of the nervous system [11]. In fact, the US Environmental Protection Agency (USEPA) and the International Agency of Research on Cancer (IARC) classified MTBE as a potential human carcinogen [12, 13].

Due to the various environmental and health implications of MTBE environmental contamination, different treatment and remediation strategies have been developed for its removal. Common examples of the technique employed include; adsorption, air stripping, bio-remediation and advanced oxidation processes (AOPs) [2, 14–17]. In recent years, the AOPs have emerged as an effective strategy for the treatment of MTBE. The AOPs involve the production of the hydroxyl radicals ($\cdot\text{OH}$) of extreme oxidation potential that disrupt the structure and the bonds of the target analyte (organic compound) and eventually mineralizes it into harmless products mainly carbon dioxide and water [18]. This oxidation process can be initiated by photolysis (O_3/UV) [19], ($\text{UV}/\text{H}_2\text{O}_2$) [20], Fenton process [8] and photocatalysis [21]. The other remediation techniques mentioned above have been reported to have certain limitation(s) when it comes to MTBE. For instance, adsorption has the advantage of generating little or no harmful by-products, but its performance in removing MTBE is limited by the fact that the saturated adsorbents are not regenerable [16, 22, 23]. Also, air stripping is cheap to operate and has been successfully applied to remediate many VOCs. However, the inherently low Henry's Law constant of MTBE heightens the air–water ratio and residence time thereby reducing the air stripper's efficiency [2]. Lastly, the bioremediation is a slow process that takes months which renders it less effective in the treatment of MTBE.

It is important to point out that photocatalytic oxidation has a high reaction rate which is suitable for better treatment of MTBE. Several important studies have been undertaken towards photocatalytic decomposition of MTBE using TiO_2/UV [24–30]. It is remarkable to highlight that these referenced studies revealed that a host of reaction conditions (such as catalyst dose, solution pH, initial pollutant concentration, irradiation UV wavelength and treatment time) influence the efficiency of MTBE degradation through the photocatalytic process. Practically, investigating all the various environmental conditions is uneconomical, time-consuming and laborious. In the same token, empirical modeling is quite challenging due to the multifactorial and complex nonlinear nature of the

problem. Consequently, researchers tend to select subjectively parameters' values (especially initial MTBE concentrations) to work with based on their available reactor systems (batch, slurry, commercial reactor or self-designed system), their analytical instrument capability and sensitivity (injection system and GC detector type), and/or prior experimental experience [24, 25, 27, 31, 32]. As a result, a wide range of differing optimal experimental conditions is reported which makes systematic studies of optimal photocatalysis conditions very challenging [2]. Therefore, the development of a computational model that can examine the effect of the above-mentioned factors becomes highly necessary towards reducing the experimental burdens encountered while finding optimal conditions for the degradation of MTBE using TiO_2 as a photocatalyst.

So far, in pursuit of this goal, only a few studies have attempted to model photolytic AOP conditions using computational intelligent approaches. Few important examples include the development of an artificial neural network (ANN) model for the evaluation of MTBE concentration degradation using $\text{UV}/\text{H}_2\text{O}_2$ by Salari et al. [33]. Also, Vaferi et al. [34] used ANN to model the photolytic treatment of MTBE and related aromatic hydrocarbons. Meanwhile, a computational approach called support vector regression (SVR) has been shown to have better prediction capability than ANN and adaptive neuro-fuzzy inference system (ANFIS) for some problems [35]. In this contribution, we investigated the influence of TiO_2 as a photocatalyst on the treatment of MTBE under various experimental conditions using the SVR model. TiO_2 is a well-studied photocatalyst for the treatment of organic contaminants [19]. However, to the best of our knowledge, modeling the performance of TiO_2 on MTBE under various experimental conditions has not been undertaken. The proposed model was developed using as inputs, 5 important factors which include; solution pH, TiO_2 dose, initial MTBE concentration, UV wavelength and contact time. The proposed model exhibits a high correlation coefficient and low maximum absolute error of 98.3% and 0.02, respectively, which clearly indicates the reliability of the model. More importantly, the optimum experimental conditions for degradation efficiency of MTBE using TiO_2 was established.

2 Description of the proposed support vector regression

2.1 Brief descriptions of SVM theory

The conceptual framework of Support Vector Machine (SVM) was founded by Vapnik [36]. Since its introduction, there have been increasing interests in the use of SVM

across diverse fields of studies [37–42]. Originally, SVM was developed for classification tasks but was later extended to regression problems [43]. SVM used for classification is referred to as support vector classification (SVC) while SVM used for regression task is termed support vector regression (SVR) [36]. SVR was developed on the basis of structural risk minimization, which makes it to have improved generalization ability compared to the artificial neural network and partial least squares that are based on empirical risk minimization [36]. In SVR, the input data is mapped into higher dimensional feature space by using a kernel function that allows the linear and non-linear problems to be solved by a linear regression function.

Assuming we have training dataset defined by $\{(x_1, y_1), \dots, (x_n, y_n)\} \subset \mathcal{X} \times \mathbb{R}$ where \mathcal{X} denotes the space of the input patterns, for example, $\mathcal{X} = \mathbb{R}^d$. In SVR, the main goal is to find a function $f(x)$ that does not have more than ϵ deviation from the real value of targets (y_i) for all the training data and such function should be as flat as possible [19, 44]. Simple case of a linear function is described by

$$f(x) = \langle w, x \rangle + b \quad \text{with } w \in \mathcal{X}, b \in \mathbb{R} \tag{1}$$

where $\langle \cdot, \cdot \rangle$ is the dot product in \mathcal{X} , $y(x)$ is the target variable, x is the input vector which consists of the design variables, w is the weight vector and b is the intercept vector. In order for the function to be flat as stated, w is required to be small, which necessitates the minimization of Euclidean norm i.e. $|w|^2$.

This can be stated as convex optimization problem and the condition is given below:

$$\begin{aligned} &\text{minimize } \frac{1}{2} \|w\|^2 \\ &\text{subject to } \begin{cases} y_i - w, x - b \leq \epsilon \\ w, x + b - y_i \leq \epsilon \end{cases} \end{aligned} \tag{2}$$

The above holds if function f exists whereby all pairs of (x, y_i) are approximated with a precision, ϵ . In reality, some errors are introduced that violate the above condition. To deal with this, slacked variables ξ_i and ξ_i^* were introduced to take care of the impractical constraints of the optimization problem as shown below [45]

$$\begin{aligned} &\text{minimize } \frac{1}{2} \|w\|^2 + C \sum_{i=1}^l (\xi_i + \xi_i^*) \\ &\text{subject to } \begin{cases} y_i - w, x - b \leq \epsilon + \xi_i \\ w, x + b - y_i \leq \epsilon + \xi_i^* \\ \xi_i, \xi_i^* \geq 0 \end{cases} \end{aligned} \tag{3}$$

where C is a non-negative constant, referred to as box constraint. It controls data points that lie beyond the

ϵ -insensitive loss margin and also useful in preventing overfitting [46]. Small values of C lead to flat functions while higher values may result in overfitting problem.

The quadratic optimization problem above can be solved by constructing the Lagrangian (L) from (3) as shown below

$$\begin{aligned} L = \frac{1}{2} \|w\|^2 + C \sum_{i=1}^l (\xi_i + \xi_i^*) - \sum_{i=1}^l \alpha_i (\xi + \xi_i - y_i + (w, x_i) + b) \\ - \sum_{i=1}^l \alpha_i^* (\xi + \xi_i^* + y_i - (w, x_i) - b) - \sum_{i=1}^l (\eta_i \xi_i + \eta_i^* \xi_i^*). \end{aligned} \tag{4}$$

where η_i^* , η_i , α_i and α_i^* are the Lagrange multipliers which are non-negative real numbers

By taking the partial derivatives of the variable L with respect to these variables (ξ_i , ξ_i^* , b , w) in (4), and then setting the results to zero for optimality condition, we obtained dual optimization problem in (5). More details of the derivation is contained in the references [47–49].

$$\begin{aligned} &\text{maximize } \begin{cases} \frac{1}{2} \sum_{i=1}^l (\alpha_i - \alpha_i^*) (\alpha_j - \alpha_j^*) (x_i, x_j) \\ -\epsilon \sum_{i=1}^l (\alpha_i + \alpha_i^*) + \sum_{i=1}^l y_i (\alpha_i - \alpha_i^*) \end{cases} \\ &\text{subject to } \sum_{i=1}^l (\alpha_i - \alpha_i^*) = 0 \text{ and } \alpha_i, \alpha_i^* \in [0, C] \end{aligned} \tag{5}$$

From the above derivatives, the value of

$$w = \sum_{i=1}^l (\alpha_i^* - \alpha_i) x_i \tag{6}$$

It follows that the objective function $y(x)$ can be expressed as shown in (7) as

$$y(x) = \sum_{i=1}^l (\alpha_i^* - \alpha_i) x_i, x + b \tag{7}$$

The b value is evaluated from the Karush–Kuhn–Tucker (KKT) conditions [49]. The above treatment is for linear problems. However, it can be extended to nonlinear function by simply transforming the training patterns x_i into some feature space, then apply Eq. 7 to the transformed x_i patterns. This leads to a new expression for the weight and the objective function

$$w = \sum_{i=1}^l (\alpha_i^* - \alpha_i) \varphi(x) \tag{8}$$

The actual objective function then takes the form of

$$f(x) = \sum_{i=1}^l (\alpha_i^* - \alpha_i) x_i + b \tag{9}$$

where $K(x_i, x)$ is the kernel parameter that transforms non-linear function into higher dimensional space.

Examples of common kernel parameters include:

- Gaussian or radial basis function (RBF): $K(x_i, x_j) = \exp(-\gamma |x_i - x_j|^2)$.
- Linear; $K(x_i, x_j) = (x_i, x_j)$
- Polynomial; $K(x_i, x_j) = [\gamma \cdot (x_i, x_j) + 1]^d, \gamma > 0$

In this study, we employed the radial basis function due to its ability to give excellent results.

3 Methodology

3.1 Sources and description of the data

The experimental data used in this study were collected from nine (9) different literature sources listed in Table 1 with their details. In the experiments, synthetic MTBE contaminated water was prepared from 97 to 99.9% pure MTBE and, treated with specific doses of anatase TiO_2 in a batch [25, 28, 30] or slurry photocatalytic reactor system equipped with UV lamps [24, 29]. The pH of

the contaminated water was adjusted using 0.1 N NaOH or 0.1 N HCl [26]. The degradation reaction was allowed to run for a specified time from zero to a maximum of 360 min (see Table 1). Initial and final MTBE concentrations in the solution were analyzed using gas chromatography (GC) equipped with either a flame ionization detector (FID) [28, 29, 50] or mass spectrometer (MS) [25, 27, 30]. During the analysis, samples are injected on to the GC via headspace [26, 28, 30, 31], purge and trap [24, 25] or solid-phase micro extraction (SPME) technique [27]. These sample injection methods are suitable for highly volatile water-soluble VOCs like MTBE. The degradation efficiency of the photocatalytic treatment was evaluated using the equation:

$$Degradation\ Efficiency(\%) = [(C_o - C_f)/C_o] \times 100\% \tag{10}$$

where C_o and C_f are initial and final MTBE concentrations respectively.

3.2 Statistical analysis of the datasets

Table 2 shows the basic statistics of the five input variables used in building the SVR model. The wide differences in the values of the mean and median of all the independent variables suggest that the sample data are not normally distributed. The standard deviation, mean and the range values also give an indication of wide variations in the data of all the parameters. In particular, the standard deviation

Table 1 Sources and details of the experimental data used for building the SVR model

Sample size (n)	pH	Catalyst dose (g/L)	UV wavelength (nm)	Initial MTBE concentration (ppm)	Contact time (mins)	% degradation efficiency	Refs.
10	7	2	254–365	0.5	0–120	0.0–95.8	[30, 31]
105	1–11	1.5–5	254–365	8.8–106	0–120	0.0–100	[28]
1	7	0.02	254	4.0	30.0	99.9	[27]
21	7	0.01–0.1	320	0.38–1	0–90	0.0–99.9	[24]
76	4–9	0.8–4.8	315	10–500	0–150	0.0–100	[26, 50]
13	6.8	0.125	300	88.15	0–360	0.0–100	[25]
23	7	0.25–5	333	1007–1460	0–240	0.0–98.4	[29]

Table 2 Basic statistics of the independent variables and their correlations with degradation efficiency

Variable	Unit	Mean	Minimum	Maximum	Standard deviation	Standard error	Correlation (r) with dependent variable
Solution pH	–	5.21	1.00	11.00	1.95	0.12	0.24
TiO_2 dose	g/L	2.06	0.00	5.00	1.26	0.08	–0.10*
Initial MTBE concentration	ppm	198.33	0.38	1460	315.22	19.98	–0.05*
UV wavelength	nm	293.23	254.00	365	35.35	2.24	0.23
Contact time	mins	44.90	0.00	360	46.03	2.92	0.61

*Not significant at a p value of 0.05

of initial MTBE concentration is notably more (by almost twice) than the mean value. This wide variation is due to the detection limits of the analytical instruments used in measuring the MTBE concentration. In other words, while GCMS is capable of accurately measuring MTBE concentration from a very low sub-ppb range up to low ppm range, reliable results are obtainable from GCFID only in the low ppb to ppm range [51]. Our data come from researches that used both types of GC detectors. Hence, the wide dispersions are expected. Nevertheless, normally distributed datasets have better prediction ability than otherwise [40]. We, therefore, normalized the datasets to manage the wide dispersion using the equation;

$$X_{new} = \frac{X - X_{min}}{X_{max} - X_{min}} \quad (11)$$

The relationships between each of the independent variables and the target were investigated by finding their Pearson product-moment correlation coefficients (r). The values of r show that the predictors with significant correlations have positive relationships with the target. In contrast, catalyst dose and contaminant initial concentration have a negative and non-significant relationship with the dependent variable. The implication of this observation is that these two parameters are possibly poor predictors of our output. In fact, traditional regression would likely exclude these parameters. Experimentally however, the solution pH and initial concentration indeed have a somewhat strong relationship with the degradation efficiency of the photo-catalysis. Moreover, one of the strengths of computational methods and SVR in particular is the ability to utilize hidden and nonlinear relationships (which traditional statistics may overlook) to make accurate predictions [35].

3.3 Computational methodology and SVR parameter optimization

We carried out the computational processing using MATLAB, version R2015b. Libsvm, a Matlab tool-box containing the necessary SVR function for the model development and simulation, was used. The data were normalized prior to data training to enhance computational efficiency. The 249 experimental data were divided randomly into two portions, namely; training and testing datasets. The training dataset (224 datapoints) was used to develop the SVR model, while the remaining were used as testing datasets to validate the performance of the model. We applied 10-fold test-set-cross validation for the model development. The prediction accuracy of the proposed SVR model depends on selecting the optimum values of the SVR turning parameters. In our case, the four (4) SVR model parameters that modulate support vector learning system

Table 3 Optimized SVM parameters

Parameter	Optimized value
C	800
Lambda	5×10^{-5}
Epsilon	2.85
K-option	0.142
Kernel function	RBF

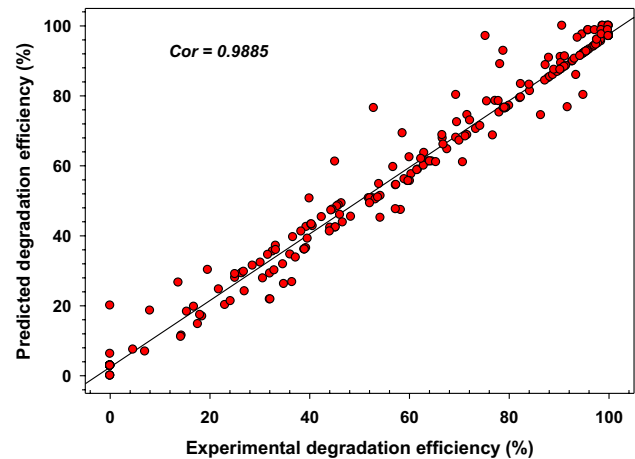


Fig. 1 Correlation plot between experimental and SVR predicted results for the photocatalytic degradation efficiency of MBTE in the presence of TiO_2 as the photocatalyst (training data)

include C , λ , k -option and ϵ . Each of the parameters was separately optimized. For example, for the optimization of C , the values of λ , ϵ and k -option were kept constant while C is varied. The values of the coefficient of correlation (CC) and the root mean square error (RMSE) were monitored during each computational run. The value of C (regularization parameter) that gives the highest coefficient of correlation and the lowest RMSE was taken as the optimized C value. The approach is repeated for other parameters and the final SVR optimized parameters are presented in Table 3 and Figures S1–S4.

4 Results and discussions

4.1 Validation of the SVR model

Figures 1 and 2 are the correlation plots used to compare the values of SVR predicted degradation efficiency and their corresponding experimental values. The correlation coefficients (r) of the regression lines of fit (shown in the plots) are 0.9885 and 0.9828 for training and testing datasets respectively. A good model has the value of r closer to 1, whereas if the value of r is closer to 0, the model is poor.

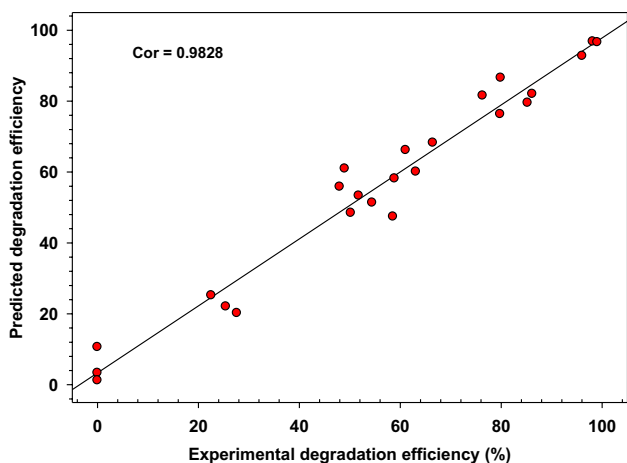


Fig. 2 Correlation plot between experimental and SVR predicted results for the photocatalytic degradation efficiency of MBTE in the presence of TiO₂ as the photocatalyst (testing data)

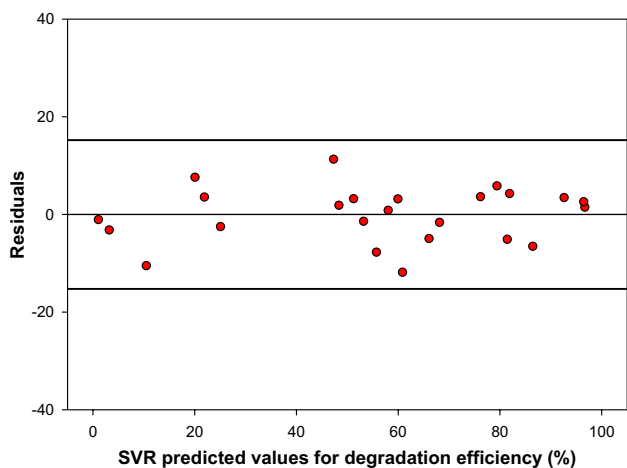


Fig. 3 Distribution of residuals from the predicted values of MTBE photodegradation efficiency using testing dataset

The proposed SVR model is therefore suitable for modeling the photocatalytic degradation of MTBE since the values of 'r' are close to unity. Moreover, since the regression line of fit is assumed linear, it is essential to examine the randomness of the error term in order to confirm the model's validity. The residual plot of testing data (Fig. 3) shows that the data are well dispersed around the zero line and, has no particular pattern. These further affirms the validity of the SVR model.

4.2 Evaluation of prediction capability of the proposed model

After establishing the validity of the model, we investigated its prediction capability in terms of accuracy. We

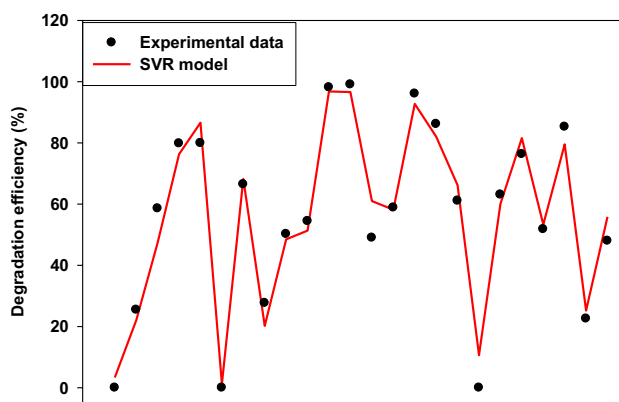


Fig. 4 Comparison of the experimental and SVR model prediction for degradation efficiency of MBTE in the presence of TiO₂

Table 4 Estimation of model reliability using estimates of errors

	Training	Testing
Correlation	0.988505	0.982767
RMSE	5.069307	5.535019
MAE	0.002292	0.021592

compared the experimental testing data with the SVR predicted results from testing data to check the model's accuracy. As shown in Fig. 4, the SVR model correctly predicts the pattern and points of the experimental data. This close match confirms the accuracy of the SVR model. Even though the model line deviates slightly from a few experimental points, the deviation still falls within acceptable experimental error. Still, the estimation of this error gives information about the reliability of the model. The statistical parameters used for the evaluation of the model's prediction ability include the root mean square error, mean absolute error and the Pearson's correlation coefficient. These indices are expressed mathematically in Eqs. (12–14). Table 4 shows the correlation coefficients and error estimates obtained during the training and testing phase of the model development. The RMSE obtained for both training and testing datasets are less than 6% and fall within the analytical QC acceptable criteria which could be up to 20% [52]. Similarly, the MAE values obtained are very small. These confirm the accuracy and reliability of the proposed SVR model.

$$RMSE = \sqrt{\frac{1}{n} \left\{ \sum_i^n (D_{e(pr)} - D_{e(ex)})^2 \right\}} \tag{12}$$

$$MAE = \frac{\sum_i^n |D_{e(pr)} - D_{e(ex)}|}{n} \tag{13}$$

$$r = \frac{\sum_i^n (D_{e(ex)} - \overline{D_{e(ex)}}) ((D_{e(pr)} - \overline{D_{e(pr)}}))}{\sqrt{\sum_i^n (D_{e(ex)} - \overline{D_{e(ex)}})^2 ((D_{e(pr)} - \overline{D_{e(pr)}}))^2}} \quad (14)$$

where n is the total number of the dataset. $D_{e(ex)}$ and $D_{e(pr)}$ refers to the experimental and the predicted values of degradation efficiency, respectively. While $\overline{D_{e(ex)}}$ and $\overline{D_{e(pr)}}$ refer to their respective mean.

4.3 Effects of experimental input variables on MTBE degradation

As mentioned earlier, five experimental parameters were considered as independent variables in building the SVR model. These parameters influence MTBE photocatalysis differently. It is, therefore, imperative to study how they affect the photocatalytic process. We compared the SVR model with experimental data and used graphical representation to investigate their effects on MTBE photo degradation.

4.4 Effect of catalyst dosage

Figure 5 summarizes the influence of catalyst dosage on the degradation of MTBE in wastewater. The SVR model accurately captures the experimental observations. Although the model appears to slightly underestimate the observed data at dosages beyond 2.4 g/L, the difference is not significant and, probably, the model results are approximation of experimental/instrumental errors that could not be detected during the experiments. As shown in the figure, the optimum dosage is around 2.4 g/L. Lower dosages (< 2 g/L) are not enough for generation of

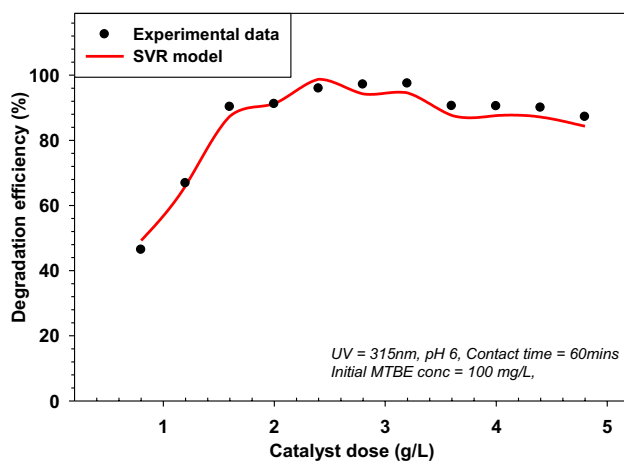


Fig. 5 Effect of TiO_2 dose on the photocatalytic degradation efficiency of MTBE

sufficient hydroxyl radicals. In addition, dosages above the optimum do not result in any significant improvement in MTBE degradation. It is important to mention that both UV and catalyst must be present before photo-degradation can occur. This is because TiO_2 does not adsorb MTBE significantly and MTBE is inert to UV radiation [30, 53–56]. The mechanism of photo-degradation is such that the photons of UV light generate energy greater than 3.2 eV which is enough to excite an electron (e^-) in the valence band of TiO_2 semiconductor, promoting it to the conduction band and leaving a positive hole behind. The e^- in the conduction band rapidly reduces the adsorbed water on TiO_2 surface into hydroxyl radicals while the positive hole oxidizes the water and converts to $\cdot\text{OH}$ radicals. Insufficient amount of the semiconductor photo-catalyst translates to short supply of $\cdot\text{OH}$ radicals and eventually results in poor degradation efficiency. Therefore, it is important to have a good dose of catalyst. Conversely, if the TiO_2 is excessive, its surfaces bounce off UV radiation lowering the production of $\cdot\text{OH}$ radicals. Our SVR model gives a good estimation of these observations.

4.5 Effect of contaminated solution pH

Figure 6 shows the effect of solution pH on MTBE mineralization. The SVR model gives a good approximation of the experimental observations, implying good performance of the model. From Fig. 6, the solution at pH 3 resulted in better MTBE degradation. Two important factors account for this; first, the solubility of MTBE in water is lowest at pH 3 (as our numerous laboratory experiments show). MTBE is thereby more readily available to $\cdot\text{OH}$ radicals for degradation at around pH 3 than at any other pH values. The second factor is due to the influence of interference from inorganic species present water. Anions such as carbonate

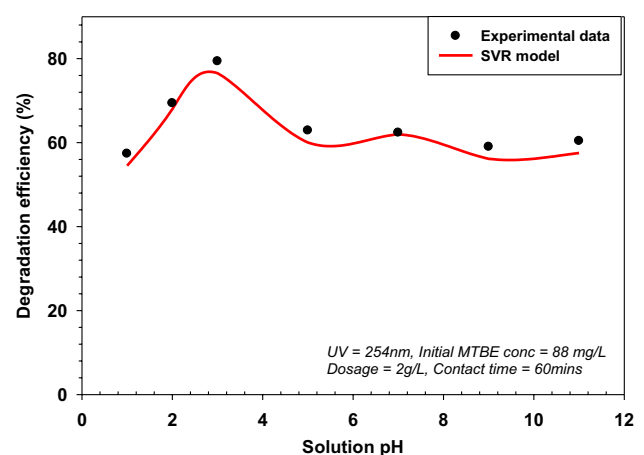


Fig. 6 Effect of solution pH on the photocatalytic degradation efficiency of MTBE in the presence TiO_2

form layer on TiO_2 surfaces hindering the photocatalytic formation of $\cdot\text{OH}$ radicals and also interfering the reactivity of inefficiently produced $\cdot\text{OH}$ radicals with MTBE [32]. This phenomenon occurs mainly at higher pH values because, at acidic pH, the anions are unstable and therefore cannot compete well with the $\cdot\text{OH}$ radicals and MTBE. Extreme low pH values such as ≤ 1.0 lead to the dissolution of TiO_2 [28] and reduced photocatalytic activity of the semiconductor.

4.6 Effect of treatment contact time

Treatment time affects the extent and kinetics of photocatalytic degradation of organic compounds. Figure 7 shows that the proposed SVR model correctly modeled the trend of the experimental data to a large extent. Importantly, the model indicates that the degradation kinetics progressed at three different rates. The reaction rate was fastest within the first 20 min, reaching a degradation efficiency rate of 2.32 percent per minutes on average. A previous study [32] showed that the production of the first intermediate product of MTBE oxidation, *tert*-Butyl formate (TBF), is peaked at 20 min of contact time. Typically, MTBE degrades to organic intermediates which are mainly *tert*-Butyl alcohol (TBA), TBF and acetone [25, 57, 58]. These products compete with MTBE for OH radicals and slow down MTBE degradation efficiency rate significantly to about 0.60 min^{-1} . During this stage, the contaminant and its intermediates are photodegraded to final products, water, and CO_2 . After 100 min, the SVR model predicted a maximum MTBE degradation efficiency of about 98%. Then, during the last stage of the quasi-static reaction rate of $\sim 0.00 \text{ min}^{-1}$, the intermediates are mineralized completely [30]. This suggests that the treatment time of 2 h is optimum for complete mineralization of MTBE and intermediates.

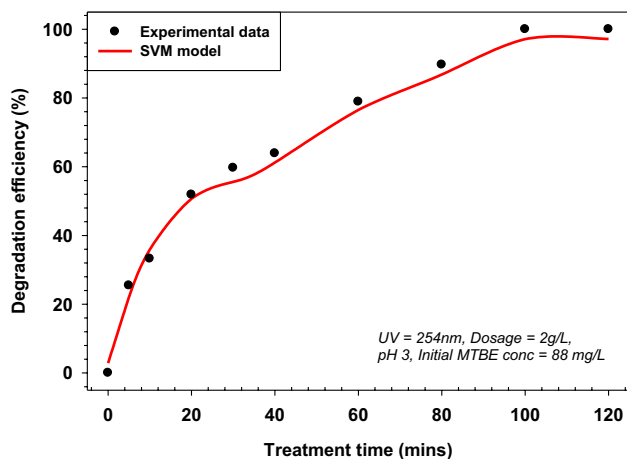


Fig. 7 Effect of reaction time on the photocatalytic degradation efficiency of MTBE in the presence of TiO_2

4.7 Effect of initial MTBE concentration

The type of GC detector used in analyses of MTBE concentrations before and after treatment limits the concentration range that researchers are able to investigate. Support vector machine (SVM) produces a global solution to problems like this. The effect of MTBE concentration on the efficiency of photo-degradation is shown in Fig. 8. From the figure, the SVR model gives an accurate estimation of the experimental observations. Under the same experimental conditions, MTBE initial concentration in water has an inverse relationship with degradation efficiency. Degradation rate, on the other hand, increases with increasing concentration [24] suggesting appreciable degradation even at high MTBE concentration. Accordingly, the proposed SVR model showed that while about 96% of up to 20 ppm MTBE can be photodegraded within 60 min, the degradation efficiency of $\sim 70\%$ is attainable within the same time when the initial MTBE concentration is high (≥ 100 ppm). It is therefore instructive to increase treatment time and/or catalyst dosage when the MTBE initial concentration is greater than 20 ppm. As discussed under the previous subsection, the contact time of 2 h could give optimal MTBE treatment.

5 Conclusion

In this study, photocatalytic degradation efficiency of Methyl *tert*-Butyl Ether (MTBE) in the presence of TiO_2 /UV as photocatalyst were accurately modeled using support vector regression model (SVR). The model was developed using as inputs the following parameters; TiO_2 dose, initial MTBE concentration, UV wavelength and contact time. The developed SVR model successfully modeled

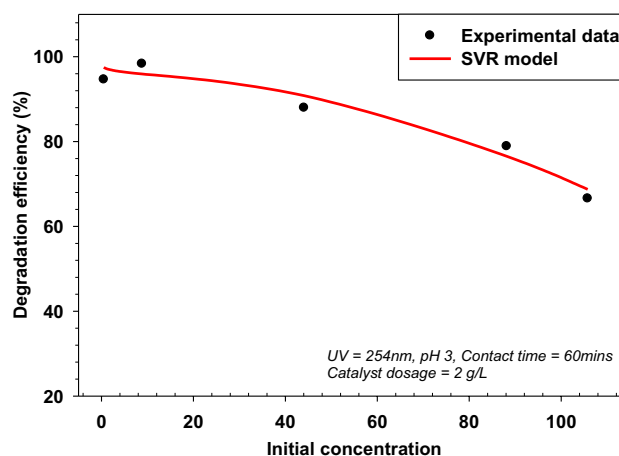


Fig. 8 Effect of initial MTBE concentration on the photocatalytic degradation efficiency of MTBE in the presence of TiO_2

the efficiencies of degrading MTBE using TiO_2/UV and under various experimental conditions. The prediction performance of the SVR model was very high as measured by correlation coefficients of 98.85% and 98.28% for training and testing dataset, respectively. Furthermore, root means square errors were calculated as 5.07% and 5.54% for training and testing dataset, respectively. More importantly, the effects of experimental conditions such as catalyst dose, solution pH, initial pollutant concentration and treatment time indicate that excellent treatment of 0.5–100 ppm MTBE-contaminated water is achievable using 2.4 g/L catalyst dose with UV radiation and maintaining a solution pH 3 and treatment time of 2 h. These computationally determined optimal experimental conditions can be useful for upscaling of photocatalysis for industrial water treatment applications.

Acknowledgements The authors acknowledge the supports received from College of Petroleum Engineering and Geosciences, and King Fahd University of Petroleum and Minerals (KFUPM), Saudi Arabia in terms of resources provided for the research.

Compliance with ethical standards

Conflict of interest The authors declare that they have no conflict of interest.

References

1. Reuter JE, Allen BC, Richards RC, Pankow JF, Goldman CR, Scholl RL, Seyfried JS (1998) Concentrations, sources, and fate of the gasoline oxygenate methyl tert-butyl ether (MTBE) in a multiple-use lake. *Environ Sci Technol* 32(23):3666–3672
2. Levchuk I, Bhatnagar A, Sillanpää M (2014) Overview of technologies for removal of methyl tert-butyl ether (MTBE) from water. *Sci Total Environ* 476–477:415–433
3. Zwank L, Schmidt TC, Haderlein SB, Berg M (2002) Simultaneous determination of fuel oxygenates and BTEX using direct aqueous injection gas chromatography mass spectrometry (DAI-GC/MS). *Environ Sci Technol* 36(9):2054–2059
4. Rossner A, Knappe DRU (2008) MTBE adsorption on alternative adsorbents and packed bed adsorber performance. *Water Res* 42(8–9):2287–2299
5. Bonjar GH (2004) Potential ecotoxicological implication of methyl tert-butyl ether (MTBE) spills in the environment. *Ecotoxicology* 13(7):631–635
6. Cassada DA, Zhang Y, Snow DD, Spalding RF (2000) Trace analysis of ethanol, MTBE, and related oxygenate compounds in water using solid-phase microextraction and gas chromatography/mass spectrometry. *Anal Chem* 72(19):4654–4658
7. Kinner NE, Director BBC, Salem NH (2001) Fate, transport and remediation of MTBE. In: Testimony before US Senat Committee Environment Public Work Salem, NH April, vol 23
8. Burbano AA, Dionysiou DD, Suidan MT (2008) Effect of oxidant-to-substrate ratios on the degradation of MTBE with Fenton reagent. *Water Res* 42(12):3225–3239
9. Moreels D, Van Cauwenberghe K, Debaere B, Rurangwa E, Vromant N, Bastiaens L, Diels L, Springael D, Merckx R, Ollevier F (2006) Long-term exposure to environmentally relevant doses of methyl-tert-butyl ether causes significant reproductive dysfunction in the zebrafish (*Danio rerio*). *Environ Toxicol Chem* 25(9):2388–2393
10. Chen CS, Hseu YC, Liang SH, Kuo JY, Chen SC (2008) Assessment of genotoxicity of methyl-tert-butyl ether, benzene, toluene, ethylbenzene, and xylene to human lymphocytes using comet assay. *J Hazard Mater* 153(1–2):351–356
11. Liab D, Liuab Q, Gongab Y, Huangc Y, Hanab X (2009) Cytotoxicity and oxidative stress study in cultured rat Sertoli cells with methyl tert-butyl ether (MTBE) exposure. *Reprod Toxicol* 27(2):170–176
12. Lewis DL, Garrison AW, Wommack KE, Whittemore A, Steudler P, Melillo J (1999) Influence of environmental changes on degradation of chiral pollutants in soils. *Nature* 401(6756):898–901
13. ATSDR (1996) Toxicological profile for Methyl tert-butyl ether (MTBE). US Department of Health and Human Services, no. 268
14. Stocking AJ, Eylers H, Wooden M, Herson T, Kavanaugh MC (2000) Treatment technologies for removal of methyl tertiary butyl ether (MTBE) from drinking water. In: Melin G (ed) National water research institute, no. February 2000. California: National Water Research Institute, p 432
15. Stasinakis AS (2008) Use of selected advanced oxidation processes (AOPs) for wastewater treatment: a mini review
16. Sutherland J, Adams C, Kekobad J (2004) Treatment of MTBE by air stripping, carbon adsorption, and advanced oxidation: technical and economic comparison for five groundwaters. *Water Res* 38(1):193–205
17. Schmidt TC, Schirmer M, Weiss H, Haderlein SB (2004) Microbial degradation of methyl tert-butyl ether and tert-butyl alcohol in the subsurface. *J Contam Hydrol* 70(3–4):173–203
18. Alansi AM, Al-Qunaibit M, Alade IO, Qahtan TF, Saleh TA (2018) Visible-light responsive BiOBr nanoparticles loaded on reduced graphene oxide for photocatalytic degradation of dye. *J Mol Liq* 253:297–304
19. Garoma T, Gurol MD, Oxidation of methyl tert-butyl ether in aqueous solution by an ozone/UV process
20. Cater SR, Stefan MI, Bolton JR, Safarzadeh-Amiri A (2000) UV/ H_2O_2 treatment of methyl tert-butyl ether in contaminated waters. *Environ Sci Technol* 34(4):659–662
21. Safari M, Nikazar M, Dadvar M (2013) Photocatalytic degradation of methyl tert-butyl ether (MTBE) by Fe-TiO₂ nanoparticles. *J Ind Eng Chem* 19(5):1697–1702
22. Liadi MA, Tawabini B, Shawabkeh R, Jarrah N, Oyehan TA, Shai-bani A, Makkawi M (2018) Treating MTBE-contaminated water using sewage sludge-derived activated carbon. *Environ Sci Pollut Res*, 1–11
23. Adebayo S, Tawabini B, Atieh M, Abuilaiwi F, Alfadul S (2016) Investigating the removal of methyl tertiary butyl ether (MTBE) from water using raw and modified fly ash waste materials. *Desalin Water Treat* 57(54):26307–26312
24. Almquist CB, Sahle-Demessie E, Enriquez J, Biswas P (2003) The photocatalytic oxidation of low concentration MTBE on titanium dioxide from groundwater in a falling film reactor. *Environ Prog Sustain Energy* 22(1):14–23
25. Barreto RD, Gray KA, Anders K (1995) Photocatalytic degradation of methyl-tert-butyl ether in TiO₂ slurries: a proposed reaction scheme. *Water Res* 29(5):1243–1248
26. Eslami A, Nasser S, Yadollahi B, Mesdaghinia A, Vaezi F, Nabizadeh R (2007) Application of photocatalytic process for removal of methyl tert-butyl ether from highly contaminated water. *Iran J Environ Heal Sci Eng* 4(4):215–222
27. Mascolo G, Ciannarella R, Balest L, Lopez A (2008) Effectiveness of UV-based advanced oxidation processes for the remediation of hydrocarbon pollution in the groundwater: a laboratory investigation. *J Hazard Mater* 152(3):1138–1145

28. Hu Q, Zhang C, Wang Z, Chen Y, Mao K, Zhang X, Xiong Y, Zhu M (2008) Photodegradation of methyl tert-butyl ether (MTBE) by UV/H₂O₂ and UV/TiO₂. *J Hazard Mater* 154(1–3):795–803
29. Kuburovic N, Todorovic M, Raicevic V, Orlovic A, Jovanovic L, Nikolic J, Kuburovic V, Drmanic S, Solevic T (2007) Removal of methyl tertiary butyl ether from wastewaters using photolytic, photocatalytic and microbiological degradation processes. *Desalination* 213(1–3):123–128
30. Tawabini BS, Atieh M, Mohyeddin M (2013) Effect of ultraviolet light on the efficiency of nano photo-catalyst (UV/CNTs/TiO₂) composite in removing MTBE from contaminated water. *Int J Environ Sci Dev* 4(2):148–151
31. Tawabini BS (2014) Removal of methyl tertiary butyl ether (MTBE) from contaminated water using UV-assisted nano composite materials. *Desalin Water Treat* 55(2):549–554
32. Mohebbali S (2013) Degradation of methyl t-butyl ether (MTBE) by photochemical process in nanocrystalline TiO₂ slurry: mechanism, by-products and carbonate ion effect. *J Environ Chem Eng* 1(4):1070–1078
33. Salari D, Daneshvar N, Aghazadeh F, Khataee AR (2005) Application of artificial neural networks for modeling of the treatment of wastewater contaminated with methyl tert-butyl ether (MTBE) by UV/H₂O₂ process. *J Hazard Mater* 125(1–3):205–210
34. Vaferi B, Bahmani M, Keshavarz P, Mowla D (2014) Experimental and theoretical analysis of the UV/H₂O₂ advanced oxidation processes treating aromatic hydrocarbons and MTBE from contaminated synthetic wastewaters. *J Environ Chem Eng* 2(3):1252–1260
35. Baghban A, Kahani M, Nazari MA, Ahmadi MH, Yan W-M (2019) Sensitivity analysis and application of machine learning methods to predict the heat transfer performance of CNT/water nanofluid flows through coils. *Int J Heat Mass Transf* 128:825–835
36. Ghorbani M, Zargar G, Jazayeri-Rad H (2016) Prediction of asphaltene precipitation using support vector regression tuned with genetic algorithms. *Petroleum* 2(3):301–306
37. Kumar KA, Ratnam C, Rao KV, Murthy BSN (2019) Experimental studies of machining parameters on surface roughness, flank wear, cutting forces and work piece vibration in boring of AISI 4340 steels: modelling and optimization approach. *SN Appl Sci* 1(1):26
38. Nguyen H (2019) Support vector regression approach with different kernel functions for predicting blast-induced ground vibration: a case study in an open-pit coal mine of Vietnam. *SN Appl Sci* 1(4):283
39. Veeragavan RK, Nivedya MK, Mallick RB (2019) Accurate identification of pavement materials that are susceptible to moisture damage with the use of advanced conditioning and test methods and the use of machine learning techniques. *SN Appl Sci* 1(1):79
40. Oyehan TA, Alade IO, Bagudu A, Sulaiman KO, Olatunji SO, Saleh TA (2018) Prediction of the refractive index of haemoglobin using the hybrid GA-SVM approach. *Comput Biol Med* 98(April):85–92
41. Sajan KS, Kumar V, Tyagi B (2015) Genetic algorithm based support vector machine for on-line voltage stability monitoring. *Int J Electr Power Energy Syst* 73:200–208
42. Alade IO, Oyehan TA, Popoola IK, Olatunji SO, Aliyu B (2017) Modeling thermal conductivity enhancement of metal and metallic oxide nanofluids using support vector regression. *Adv Powder Technol*
43. Ahmadi MH, Ahmadi MA, Nazari MA, Mahian O, Ghasempour R (2018) A proposed model to predict thermal conductivity ratio of Al₂O₃/EG nanofluid by applying least squares support vector machine (LSSVM) and genetic algorithm as a connectionist approach. *J Therm Anal Calorim* 0123456789
44. Alade IO, Rahman MAA, Saleh TA (2019) Modeling and prediction of the specific heat capacity of Al₂O₃/water nanofluids using hybrid genetic algorithm/support vector regression model. *Nano-Struct Nano-Objects* 17
45. Alade IO, Rahman MAA, Saleh TA (2019) Predicting the specific heat capacity of alumina/ethylene glycol nanofluids using support vector regression model optimized with Bayesian algorithm. *Sol Energy* 183:74–82
46. Kojić P, Omorjan R (2017) Predicting hydrodynamic parameters and volumetric gas–liquid mass transfer coefficient in an external-loop airlift reactor by support vector regression. *Chem Eng Res Des* 125:398–407
47. Alade IO, Bagudu A, Oyehan TA, Rahman MAA, Saleh TA, Olatunji SO (2018) Estimating the refractive index of oxygenated and deoxygenated hemoglobin using genetic algorithm—support vector machine approach. *Comput Methods Programs Biomed*
48. Basak D, Pal S, Patranabis DC (2007) Support vector regression. *Neural Inf Process Lett Rev* 11(10):203–224
49. Smola AJ, Schölkopf B (2004) A tutorial on support vector regression. *Stat Comput* 14(3):199–222
50. Eslami A, Nasserli S, Yadollahi B, Mesdaghinia A, Vaezi F, Nabizadeh R (2009) Removal of methyl tert-butyl ether (MTBE) from contaminated water by photocatalytic process. *Iran J Public Health* 38(2):18–26
51. Agency for Toxic Substances and Disease Registry (ATSDR) (1996) Analytical Methods. In: Toxicological profile for methyl tert-butyl ether, Atlanta, GA, pp 191–198
52. USEPA (2016) Protocol for review and validation of new methods for regulated organic and inorganic analytes in wastewater under EPA's alternate test procedure program. Washington, DC 20460
53. Pengyi Z, Fuyan L, Gang Y, Qing C, Wanpeng Z (2003) A comparative study on decomposition of gaseous toluene by O₃/UV, TiO₂/UV and O₃/TiO₂/UV. *J Photochem Photobiol A Chem* 156(1–3):189–194
54. Sahle-Demessie E, Richardson T, Almquist CB, Pillai UR (2002) Comparison of liquid and gas-phase photooxidation of MTBE: synthetic and field samples. *J Environ Eng* 128(9):782–790
55. Tiburtius ERL, Peralta-Zamora P, Emmel A (2005) Treatment of gasoline-contaminated waters by advanced oxidation processes. *J Hazard Mater* 126(1–3):86–90
56. Zang Y, Farnood R (2005) Photocatalytic decomposition of methyl tert-butyl ether in aqueous slurry of titanium dioxide. *Appl Catal B Environ* 57(4):275–282
57. Stefan MI, Mack J, Bolton JR (2000) Degradation pathways during the treatment of methyl tert-butyl ether by the UV/H₂O₂ process. *Environ Sci Technol* 34(4):650–658
58. Huang K-C, Couttenye RA, Hoag GE (2002) Kinetics of heat-assisted persulfate oxidation of methyl tert-butyl ether (MTBE). *Chemosphere* 49(4):413–420

Publisher's Note Springer Nature remains neutral with regard to jurisdictional claims in published maps and institutional affiliations.